Smart Structures and Systems, *Vol. 34, No. 4 (2024) 271-282*
https://doi.org/10.12989/sss.2024.34.4.271

Semi-active control of building structures under seismic action with faulty MR dampers and sensors

Pegah Naderpoor Shad and Touraj Taghikhany*

Department of Civil Engineering, Amirkabir University of Technology, Tehran, Iran

(*Received December 11, 2022, Revised August 27, 2024, Accepted November 28, 2024*)

Abstract. In semi-active control of structures, sensors and dampers may fail in earthquake. Sensor malfunctioning mostly causes a constant offset in true signals and shifts the mean value of the recorded parameters, but a fault in a damper may reduce its effectiveness and change the mean and variance of the force that should be applied. To date, many studies have investigated the fault effect on control devices. They have mainly focused on the faults that affect the signals' mean values (additive fault). However, some faults may also change their variance (multiplicative fault). These faults' identification and control require a different strategy. This study introduces a newly designed active fault-tolerant control system (AFTCS) to identify and accommodate simultaneous multiplicative damper fault and additive sensor fault during earthquake. To do that, by dividing the structure into two subsystems, sensor and damper fault effects are separated. Then, by designing an observer based on dynamic neural network (DNN) for each subsystem, faults on control devices are estimated. Later, the true responses of the structure are obtained and finally, the proposed fault-tolerant controller accommodates damper fault effects. The AFTCS's performance was validated for different fault scenarios in a three-story building structure with magneto-rheological (MR) dampers.

Keywords: active fault-tolerant control system; DNN-based observer; multiplicative and additive faults; seismic control of structures; simultaneous sensor and damper faults

1. Introduction

Active and semi-active control systems usually include sensors, actuators, dampers, and wiring (Lin *et al*. 2018, Bozorgvar and Zahrai 2019, Chen *et al*. 2021) that failure may occur in one or more of them. Various factors cause damper faults, such as reduction of oil pressure, mechanical factors, loosening connection. In civil structures, one of the most frequent dampers is MR damper and its common fault is oil leakage that occurs due to improper installation or overuse (Xu *et al*. 2000, Li and Li 2019). Its consequence is the loss of the damping force and the damper's capacity (Jung *et al*. 2003, Tudon-Martinez and Morales-Menendez 2015). Another possible fault is the entrapment of MR fluid's magnetic particles in the piston headspace, which occurs if the damper is subjected to prolonged loading and long cycles. This fault leads to an increase in the damper output and the damper capacity at high speeds (Utami *et al*. 2018).

Noise in sensor output signals is normal and unavoidable, but high noise indicates a sensor malfunctioning that is caused by a weak battery or hardware problems (Sharma *et al*. 2007, Ni *et al*. 2009). One of the common faults of the sensors is bias or shift fault which is a constant offset in the actual signal that can occur due to incorrect calibration (Sharma *et al*. 2007, Balzano and Nowak 2007, Ni *et al*. 2009). Another frequent defect in sensors is called outlier fault where the output jumps abnormally from its true value at some points (Ramanathan *et al*. 2006).

In the literature, to maintain system stability in case of a fault in control tools and prevent the imperfection spread, fault-tolerant control systems (FTCSs) are introduced. These systems are divided into passive and active classes. An active FTCS (AFTCS) detects and accommodates the fault effects online and it keeps the system stable for a wider range of faults. The most studied faults can be classified into un-modeled and modeled faults (UMFs, MFs). A specific model cannot accurately mention UMFs. However, MFs are described as multiplicative and/or additive faults (Fig. 1). The fault in actuators can be written as $u_f = g_f u + b_f$, where u is the controller's recommended signal, u_f is the faulty damper force, $0 < g_f \leq 1$ represents the degradation of power fault (loss of effectiveness, multiplicative, or gain fault) which changes the mean and variance of the correct signal. b_f is the limited additive (bias) fault that only changes the true signal's mean. The effects of the most faults on the performance of control tools can be modeled and described by multiplicative and/or additive forms (Ossmann and Varga 2013, Shen *et al*. 2017).

Fig. 2 exhibits the generated force of a healthy MR damper for a voltage of 6 V against 2.0 Hz sinusoidal action with an amplitude equal to 10 mm. It compares the effects of the bias and multiplicative faults on this force. In Fig. 2(a), the healthy damper output is shifted as much as 6000 N which is equal to half of the maximum capacity. in Fig. 2(b), the damper loses half of its efficiency. As shown in

*Corresponding author, Ph.D., Associate Professor,
E-mail: ttaghikhany@aut.ac.ir

ISSN: 1738-1584 (Print), 1738-1991 (Online)

(a) Additive fault (b) Multiplicative fault

Fig. 1 Fault types

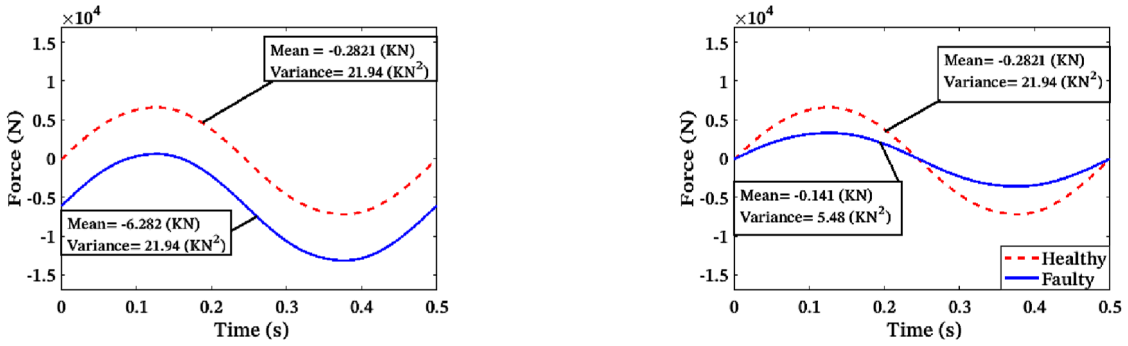

(a) Additive (bias) fault (b) Multiplicative (gain) fault

Fig. 2 MR damper force in healthy and faulty cases

this figure, the bias fault only changes the mean of the healthy damper's force, but the multiplicative fault also affects its variance.

Most studies in the FTCS literature have considered faults in only dampers or sensors. Talebi and Khorasani proposed a fault detection and isolation (FDI) method to approximate the gain fault of the actuators used for a satellite. In the method, a dynamic neural network (DNN) is responsible for guessing the fault and its convergence speed is about 50 seconds (Talebi and Khorasani 2012). However, the algorithms used to control the civil structures against ground motion excitation should converge much faster due to the short time duration of an earthquake. Zhu *et al*. took actuator faults in their control scheme. They designed an AFTCS that compensates the fault effects in the frequency domain and maintains the acceptable performance level of the building structure (Zhu *et al*. 2015). Hosseini *et al*. used the simple adaptive control method for controlling a building structure with unknown structural damages and sensor faults in earthquake (Hosseini *et al*. 2018). Naderpoor Shad and Taghikhany proposed an AFTCS for simultaneous additive faults in the sensors and the dampers (Naderpoor Shad and Taghikhany 2022). In practice, most common faults in sensors can mainly be assumed in additive form. However, a primary type of fault in dampers takes action as a multiplicative term on the control signal. The stability study and the convergence analysis of the strategy for the multiplicative fault detection and isolation are more challenging. It is because of strong coupling between the structure and the observer states. More, a change occurs in the spectral characteristics of the actual signal (Talebi and Khorasani 2012).

This paper proposes an AFTCS that tolerates the simultaneous multiplicative damper fault and additive sensor fault. Because of coupling between the damper and sensor faults, to consider them simultaneously, their effects must be separated. So, in the beginning, the main structure is split into two subsystems: one is concerned with sensor faults and the other with damper faults. Then, to correct the wrong output signal of the faulty sensors, it is necessary to estimate the sensors' faults. Hence, for the subsystem affected by sensor faults, a DNN-based observer is designed to estimate the sensor faults and the actual structure states. Similarly, to eliminate the effects of the dampers' faults from the performance of the designed control system, an observer based on DNN is also proposed for approximating the damper faults using the second subsystem and finally, a fault-tolerant controller is designed to accommodate the estimated damper faults. Here, pre-trained weights are used to improve the convergence speed and behavior of the damper fault observer's DNN. To do that, firstly, the neural network is trained offline by using the healthy control system's behavior under series of seismic ground motions. Then, the resulting weights are used in the online FDI technique. The effectiveness of the suggested method is examined for various fault scenarios in numerical model of a three-story building structure with MR dampers.

2. The strategy's formulations

The equations of the system are as follows

$$\begin{aligned} \dot{x}(t) &= Ax(t) + Bu(t) \\ y(t) &= cx(t) + D_s\left(f_s(t, x(t), u(t))\right) \end{aligned} \tag{1}$$

where $x \in R^{2n}$, $A \in R^{2n\times 2n}$, $B \in R^{2n\times(m+1)}$, and $u \in R^{(m+1)\times 1}$ are the state vector, the system matrix, the input matrix, and the input vector, respectively. They are defined as Eq. (2). $y \in R^{p}$, $c \in R^{p\times 2n}$, and $D_S \in R^{p\times q}$ are the

output vector, the output matrix, and the matrix of the sensor fault distribution, respectively. $f_S \in R^q$ is a sensor fault vector.

$$\begin{aligned} A &= \begin{bmatrix} [0]_{n\times n} & [I]_{n\times n} \\ -[M^{-1}K]_{n\times n} & -[M^{-1}C]_{n\times n} \end{bmatrix}_{2n\times 2n} \\ B &= \begin{bmatrix} [0]_{n\times 1} & [0]_{n\times m} \\ -[G]_{n\times 1} & -[M^{-1}P]_{n\times m} \end{bmatrix} \\ &= \langle B_{1(2n\times 1)} | B_{2(2n\times m)} \rangle_{2n\times(m+1)} \\ u &= \begin{Bmatrix} \ddot{x}_g(t)_{1\times 1} \\ [f_{MR}(t)]_{m\times 1} \end{Bmatrix}_{(m+1)\times 1} \end{aligned} \tag{2}$$

In these equations, C, K, and $M \in R^{n\times n}$ are the damping matrix, the stiffness matrix, and the mass matrix, respectively. $G \in R^{n\times 1}$ is the excitation matrix, $P \in R^{n\times m}$ is the control matrix, and $f_{MR} \in R^{m\times 1}$ is the damper force vector. Here, the structure is presumed to be controllable and observable.

To separate the coupling effects of two types of faults in the sensor and the damper, the main structure is divided into two substructures such that each fault is only seen in one of them (Abdollahi 2017). In this method, an output transformation S and a state-space coordinate transformation T are considered as follows

$$\begin{aligned} z(t) &= \begin{Bmatrix} z_1 \\ z_2 \end{Bmatrix} = Sy(t) \\ h(t) &= \begin{Bmatrix} h_1 \\ h_2 \end{Bmatrix} = Tx(t) \end{aligned} \tag{3}$$

where z_1, z_2, h_1, and $h_2 \in R^{n\times 1}$ are the output vectors and the state vectors of the subsystems. T is an invertible matrix that does not transfer B. It is equal to

$$T = \begin{bmatrix} [I]_{n\times n} & [0]_{n\times n} \\ [T_3]_{n\times n} & [I]_{n\times n} \end{bmatrix} \tag{4}$$

$S = S'S_0$, where $S' \in R^{2n\times 2n}$, S and $S_0 \in R^{2n\times p}$ such that $S'S_0D_s = \begin{Bmatrix} [D_{s1}]_{n\times q} \\ [0]_{n\times q} \end{Bmatrix}$ and $S'S_0cT^{-1} = \begin{bmatrix} [C_1]_{n\times n} & [0]_{n\times n} \\ [0]_{n\times n} & [C_4]_{n\times n} \end{bmatrix}$. These transformation matrices divide the structure into two following subsystems;

<u>*Subsystem 1*</u>:

$$\begin{cases} \{\dot{h}_1\}_{n\times 1} = -T_3h_1 + h_2 \\ \{z_1\}_{n\times 1} = C_1h_1 + D_{s1}(f_s) \end{cases} \tag{5}$$

and <u>*Subsystem 2*</u>:

$$\begin{cases} \{\dot{h}_2\}_{n\times 1} = A_1h_2 + A_2h_1 - G\ddot{x}_g + [M^{-1}P][f_{MR}] \\ \{z_2\}_{n\times 1} = C_4h_2 \end{cases} \tag{6}$$

C_1 is the output matrix of subsystem 1 and D_{s1} is the sensor fault distribution matrix in the new coordinate. A_1, A_2, and f_{MR} are defined as

$$A_1 = -\left[\frac{C}{M}\right] + T_3 \tag{7}$$

$$A_2 = -\left[\frac{K}{M}\right] + \left[\frac{C}{M}\right]T_3 - T_3^2 \tag{8}$$

$$f_{MR} = diag(f_d)u \tag{9}$$

where $f_d = [f_{d1}, f_{d2}, \dots, f_{dm}]^T$ is the vector of the damper effectiveness and $0 < f_{di} \le 1$, $i = 1,2,\dots,m$. When ith damper works superbly $f_{di} = 1$ and $f_{di} = 0$ means that it fails completely. C_4 is the output matrix of subsystem 2. Note that $-T_3$ and A_1 are Hurwitz matrices.

2.1 Designing sensor fault observer

To correct output signals of damaged sensors, here, an observer is proposed for subsystem 1, which is based on DNN. This neural network with the online learning ability is able to estimate the malfunctions in sensors online (Li *et al*. 2011) and it can approximate a time-dependent and multivariable function. Eq. (10) is considered as the observer (Naderpoor Shad and Taghikhany 2022)

$$\begin{cases} \dot{\hat{h}}_1(t) = -T_3\hat{h}_1(t) + C_4^{-1}z_2(t) \\ \hat{z}_1(t) = C_1\hat{h}_1(t) + D_{s1}\hat{f}_s \end{cases} \tag{10}$$

where $\hat{f}_s$ is the estimated sensor fault vector mapped by DNN and $C_4^{-1}z_2 = h_2$. A well-designed neural network with input vector X restricted to large compact set S can estimate any continuous function F(X) on the set. Therefore, F(X) and $\hat{F}(\hat{X})$ can be presented as (Oh *et al*. 2021, Gao *et al*. 2022)

$$\begin{aligned} F(X) &= W^*\sigma(V^*X) + \varepsilon^*(X) \\ \hat{F}(X) &= \widehat{W}\sigma(\hat{V}\hat{X}) \end{aligned} \tag{11}$$

where $V^* \in R^{b1\times b}$ and $W^* \in R^{b2\times b1}$ are the ideal weights, ε^* is the limited approximation error of the neural network, $\sigma(.)$ is the hidden layer neurons' transfer function and it can be any bounded output activation function that makes certain the universal approximation theorem like a sigmoidal function as (Talebi *et al*. 2008)

$$\sigma(V^*X) = \frac{2}{1 + e^{-2V^*X}} - 1 \tag{12}$$

b is the input number, b_1 is the hidden layer neuron number, and b_2 is the output layer neuron number.

Now by considering $\hat{f}_s(X_1) = \widehat{W}_1\sigma(\hat{V}_1X_1)$, Eq. (10) can be rewritten as (Naderpoor Shad and Taghikhany 2022)

$$\begin{cases} \dot{\hat{h}}_1(t) = -T_3\hat{h}_1(t) + C_4^{-1}z_2(t) \\ \hat{z}_1(t) = C_1\hat{h}_1(t) + D_{s1}(\widehat{W}_1\sigma(\hat{V}_1X_1)) \end{cases} \tag{13}$$

By defining $\tilde{h}_1 = h_1 - \hat{h}_1$, $\tilde{z}_1 = z_1 - \hat{z}_1$, $\widetilde{W}_1 = W_1^* - \widehat{W}_1$, and $\delta_1 = W_1^*\left(\sigma(V_1^*X_1) - \sigma\left(\hat{V}_1X_1\right)\right) + \varepsilon_1^*$ and using Eqs. (5) and (13), the error dynamics is obtained as (Naderpoor Shad and Taghikhany 2022)

$$\begin{cases} \dot{\tilde{h}}_1(t) = -T_3\tilde{h}_1(t) \\ \tilde{z}_1(t) = C_1\tilde{h}_1(t) + D_{s1}\left(\widetilde{W}_1\sigma\left(\hat{V}_1X_1\right) + \delta_1\right) \end{cases} \tag{14}$$

The DNN's weights are updated as follows (Talebi *et al*. 2008)

$$\begin{aligned}\widehat{W}_1 &= -\eta_1\left(\frac{\partial J_1}{\partial \widehat{W}_1}\right) - \rho_1\|\tilde{z}_1\|\widehat{W}_1 \\ \hat{V}_1 &= -\eta_2\left(\frac{\partial J_1}{\partial \hat{V}_1}\right) - \rho_2\|\tilde{z}_1\|\hat{V}_1\end{aligned} \tag{15}$$

where J_1 is the objective function of the DNN $\left(J_1 = \frac{1}{2}\tilde{z}_1^T\tilde{z}_1\right)$ and η_1, η_2, ρ_1, and ρ_2 are the positive learning parameters. Eq. (15) gives

$$\begin{aligned}\widehat{W}_1 &= \eta_1(\tilde{z}_1^T D_{s1})^T S_1^T - \rho_1\|\tilde{z}_1\|\widehat{W}_1 \\ \hat{V}_1 &= \eta_2\left(\tilde{z}_1^T D_{s1}\widehat{W}_1 S_2\right)^T X_1^T - \rho_2\|\tilde{z}_1\|\hat{V}_1\end{aligned} \tag{16}$$

where $S_1 = \sigma\left(\hat{V}_1 X_1\right)$, $S_2 = [I]_{b1\times b1} - diag(S_1^* S_1)$, and $X_1 = \left[\hat{h}_1; h_2; h_2 + \lambda'\hat{h}_1; 1\right]$ which is a combination of the system state (Naderpoor Shad and Taghikhany 2022).

To examine the system's stability, the following Lyapunov function is used (Naderpoor Shad and Taghikhany 2022)

$$L_1 = \frac{1}{2}\tilde{h}_1^T P'\tilde{h}_1 + \frac{1}{2}tr\left(\widetilde{W}_1^T\rho_1^{-1}\widetilde{W}_1\right) \tag{17}$$

As $-T_3$ is Hurwitz, there is the positive-definite matrix $P' \in R^{n\times n}$ which is obtained from the Lyapunov equation

$$-T_3^T P' + P'(-T_3) = -Q \tag{18}$$

$Q \in R^{n\times n}$ is positive semidefinite. By deriving of Eq. (17), Eq. (19) is obtained as

$$\dot{L}_1 = -\frac{1}{2}\tilde{h}_1^T Q\tilde{h}_1 + tr\left(\widetilde{W}_1^T\rho_1^{-1}\dot{\widetilde{W}}_1\right) \tag{19}$$

and then by denoting $\dot{\widetilde{W}}_1 = l_1\tilde{z}_1 S_1^T + \rho_1\|\tilde{z}_1\|\widehat{W}_1$, $l_1 = -\eta_1 D_{s1}^T$, and substituting it into Eq. (19), one can get (Naderpoor Shad and Taghikhany 2022)

$$\begin{aligned}\dot{L}_1 = -\frac{1}{2}\tilde{h}_1^T Q\tilde{h}_1 + tr\left(\widetilde{W}_1^T\rho_1^{-1}l_1\tilde{z}_1 S_1^T\right) \\ + tr\left(\widetilde{W}_1^T\|\tilde{z}_1\|\left(W_1^* - \widetilde{W}_1\right)\right)\end{aligned} \tag{20}$$

Because the sigmoidal function is bounded and the ideal weight has a finite value, σ_{max} and W_{max}^* may be defined as maximum values of them and therefore $\|\delta_1\| \le \bar{\delta}_1$. The following inequalities hold (Naderpoor Shad and Taghikhany 2022)

$$\begin{aligned}&tr\left(\widetilde{W}_1^T\rho_1^{-1}l_1\tilde{z}_1 S_1^T\right) \le \sigma_{max}\rho_1^{-1}\left\|\widetilde{W}_1\right\|\|l_1\|\|\tilde{z}_1\| \\ &tr\left(\widetilde{W}_1^T\left(W_1^* - \widetilde{W}_1\right)\right) \le W_{max}^*\left\|\widetilde{W}_1\right\| - \left\|\widetilde{W}_1\right\|^2 \\ &\|\tilde{z}_1\| \le \|D_{s1}\|\left(\left\|\widetilde{W}_1\right\|\sigma_{max} + \bar{\delta}_1\right)\end{aligned} \tag{21}$$

and then by using Eq. (20), Eq. (21) and according to that $-T_3$ is Hurwitz so $\hat{h}_1 \to h_1$, one can write (Naderpoor Shad and Taghikhany 2022)

$$\dot{L}_1 \le -\alpha_3\left\|\widetilde{W}_1\right\|^2 + \alpha_1\left\|\widetilde{W}_1\right\| + \beta_1 \tag{22}$$

where

$$\alpha_1 = \sigma_{max}\rho_1^{-1}\|l_1\|\|D_{s1}\|\bar{\delta}_1 + W_{max}^*\|D_{s1}\|\bar{\delta}_1 \tag{23}$$

$$\begin{aligned}\alpha_2 = \sigma_{max}^2\rho_1^{-1}\|l_1\|\|D_{s1}\| \\ + W_{max}^*\sigma_{max}\|D_{s1}\| - \|D_{s1}\|\bar{\delta}_1\end{aligned} \tag{24}$$

$$\alpha_3 = \|D_{s1}\|\sigma_{max} \tag{25}$$

$$\beta_1 = \frac{4}{27}\frac{(\alpha_2 + \alpha_3)^3}{\alpha_3^2} \tag{26}$$

α_2 is positive if $\rho_1^{-1}\|l_1\| > \frac{1}{\sigma_{max}^2}\left(\bar{\delta}_1 - W_{max}^*\sigma_{max}\right)$ and the other coefficients are always positive. $\dot{L}_1$ is negative semidefinite if $\left\|\widetilde{W}_1\right\| \ge \widetilde{W}_{10} = \frac{\alpha_1 + \sqrt{\alpha_1^2 + 4\alpha_3\beta_1}}{2\alpha_3}$ so $\left\|\widetilde{W}_1\right\|$ and accordingly $\|\tilde{z}_1\|$ (from Eq. (21)) are finally limited.

Finally, the structure's true state is obtained as follows

$$x(t) = c^{-1}\left(y(t) - D_s\left(f_s\left(t, x(t), u(t)\right)\right)\right) \tag{27}$$

2.2 Designing damper fault observer

For estimating the damper effectiveness, an observer based on DNN is designed for subsystem 2 and assumed $f_d = W^*\sigma(V^*X) + \varepsilon^*(X)$ and the observer equation is

$$\begin{cases}\left\{\dot{\hat{h}}_2\right\}_{n\times 1} = A_1\hat{h}_2 + A_2\hat{h}_1 - G\ddot{x}_g + [M^{-1}P]\left[diag\left(\hat{f}_d\right)u\right] \\ \{\hat{z}_2\}_{n\times 1} = C_4\hat{h}_2\end{cases} \tag{28}$$

where $\hat{f}_d$ is the estimated damper effectiveness $\left(\hat{f}_d = \widehat{W}\sigma(\hat{V}\hat{X})\right)$. By subtracting Eq. (28) from (6), one can get

$$\begin{cases}\dot{\tilde{h}}_2 = A_1\tilde{h}_2 + A_2\tilde{h}_1 + [M^{-1}P]\left[diag\left(f_d - \hat{f}_d\right)u\right] \\ \tilde{z}_2 = C_4\tilde{h}_2\end{cases} \tag{29}$$

where $\tilde{h}_2 = h_2 - \hat{h}_2$ and $\tilde{z}_2 = z_2 - \hat{z}_2$. We have already proved that $\tilde{h}_1 = h_1 - \hat{h}_1$ converges to zero. Eq. (29) can be rewritten as

$$\begin{cases}\dot{\tilde{h}}_2 = A_1\tilde{h}_2 + [M^{-1}P]\left[diag\left(W^*\sigma(V^*X) + \varepsilon^*(X) - \widehat{W}\sigma\left(\hat{V}\hat{X}\right)\right)u\right] \\ \tilde{z}_2 = C_4\tilde{h}_2\end{cases} \tag{30}$$

Here, the update rules for the neural network weights are obtained by using a modified backpropagation strategy. Then the stability of the FDI scheme will be demonstrated. The rules for updating the neural network weights are calculated as follows (Talebi *et al*. 2008, Talebi and Khorasani 2012)

$$\dot{\widehat{W}} = -\eta_3\left(\frac{\delta J}{\delta \widehat{W}}\right) - \rho_3\|\tilde{z}_2\|\widehat{W} \tag{31}$$

$$\dot{\hat{V}} = -\eta_4\left(\frac{\delta J}{\delta \hat{V}}\right) - \rho_4\|\tilde{z}_2\|\hat{V} \tag{32}$$

where the neural network objective function is defined as $J = \frac{1}{2}\tilde{z}_2^T\tilde{z}_2$ and η_3, η_4, ρ_3 and ρ_4 are the learning rates with positive values. Calculating Eqs. (31)-(32) needs to find $\left(\frac{\delta J}{\delta \widehat{W}}\right)$ and $\left(\frac{\delta J}{\delta \hat{V}}\right)$, respectively. Firstly, let us consider some definitions as $\hat{X} = [\hat{h}_1; \hat{h}_2; \hat{h}_2 + \lambda'\hat{h}_1; 1]$, $\widetilde{W} = W^* - \widehat{W}$, $\tilde{V} = V^* - \hat{V}$, $S_3 = \sigma(\hat{V}\hat{X})$ where $\sigma(V^*X) = \frac{2}{1+e^{-2V^*X}} - 1$, and $S_4 = [I]_{b1\times b1} - diag(S_3 \times S_3)$. Now, $\left(\frac{\delta J}{\delta \widehat{W}}\right)$ and $\left(\frac{\delta J}{\delta \hat{V}}\right)$ are computed as

$$\frac{\delta J}{\delta \widehat{W}} = \frac{\delta J}{\delta \tilde{z}_2}\frac{\delta \tilde{z}_2}{\delta \hat{h}_2}\frac{\delta \hat{h}_2}{\delta(\widehat{W}S_3)}\frac{\delta(\widehat{W}S_3)}{\delta \widehat{W}} \tag{33}$$

$$\frac{\delta J}{\delta \hat{V}} = \frac{\delta J}{\delta \tilde{z}_2}\frac{\delta \tilde{z}_2}{\delta \hat{h}_2}\frac{\delta \hat{h}_2}{\delta(\widehat{W}S_3)}\frac{\delta(\widehat{W}S_3)}{\delta S_3}\frac{\delta S_3}{\delta(\hat{V}\hat{X})}\frac{\delta(\hat{V}\hat{X})}{\delta \hat{V}} \tag{34}$$

From Eq. (30), $\frac{\delta \tilde{z}_2}{\delta \hat{h}_2}$ is $-C_4$ and then by considering Eq. (28), one can have

$$\frac{\delta \hat{\hat{h}}_2}{\delta(\widehat{W}S_3)} = A_1\frac{\delta \hat{h}_2}{\delta(\widehat{W}S_3)} + [M^{-1}P]diag(u) \tag{35}$$

By rewriting Eq. (35) and assuming that $d_w = \frac{\delta \hat{h}_2}{\delta(\widehat{W}S_3)}$ (Talebi and Khorasani 2012), Eq. (36) is derived as

$$\dot{d}_w = A_1 d_w + [M^{-1}P]diag(u) \tag{36}$$

Since A_1 is Hurwitz, if u is bounded, d_w will be bounded as well. Now, Eqs. (33)-(34) are redefined as

$$\frac{\delta J}{\delta \widehat{W}} = (-\tilde{z}_2^T C_4 d_w)^T S_3^T \tag{37}$$

$$\frac{\delta J}{\delta \hat{V}} = \left(-\tilde{z}_2^T C_4 d_w \widehat{W} S_4\right)^T \hat{X}^T \tag{38}$$

By substituting Eqs. (37)-(38) into Eqs. (31)-(32) respectively, one may get

$$\dot{\widehat{W}} = \eta_3(\tilde{z}_2^T C_4 d_w)^T S_1^T - \rho_3\|\tilde{z}_2\|\widehat{W} \tag{39}$$

$$\dot{\hat{V}} = \eta_4\left(\tilde{z}_2^T C_4 d_w \widehat{W} S_2\right)^T \hat{X}^T - \rho_4\|\tilde{z}_2\|\hat{V} \tag{40}$$

To survey the stability of the FDI scheme, the weights' estimate errors are determined as

$$\dot{\widetilde{W}} = -l_3 d_w^T \tilde{z}_2 S_3^T + \rho_3\|\tilde{z}_2\|\widehat{W} \tag{41}$$

$$\dot{\tilde{V}} = -l_4 S_4^T \widehat{W}^T d_w^T \tilde{z}_2 \hat{X}^T + \rho_4\|\tilde{z}_2\|\hat{V} \tag{42}$$

and the following Lyapunov function is used

$$L = \frac{1}{2}\tilde{h}_2^T P_1 \tilde{h}_2 + \frac{1}{2}tr\left(\widetilde{W}^T\rho_3^{-1}\widetilde{W}\right) \tag{43}$$

where $l_3 = \eta_3 C_4^T$, $l_4 = \eta_4 C_4^T$, and the positive-definite matrix P_1 assuring the Lyapunov equation $A_1^T P_1 + P_1 A_1 = -Q_1$ when Q_1 is a positive-definite matrix. The time derivative of Eq. (43) leads to

$$\begin{aligned}\dot{L} = -\frac{1}{2}\tilde{h}_2^T Q_1 \tilde{h}_2 + \tilde{h}_2^T P_1\left(\left[\frac{P}{M}\right]diag\left(\widetilde{W}S_3 + \delta\right)u\right) \\ + tr\left(\widetilde{W}^T\rho_3^{-1}\dot{\widetilde{W}}\right)\end{aligned} \tag{44}$$

and δ is defined as $\delta = W^*\left(\sigma(V^*X) - \sigma\left(\hat{V}X\right)\right) + \varepsilon^*$ limited to a positive scalar constant $\bar{\delta}$. According to the following inequalities (Talebi *et al*. 2008, Talebi and Khorasani 2012)

$$\begin{aligned}&tr\left(\widetilde{W}^T\left(W^* - \widetilde{W}\right)\right) \le W_{max}^*\|\widetilde{W}\| - \|\widetilde{W}\|^2 \\ &tr\left(-l_5\widetilde{W}^T d_w^T\tilde{h}_2^T S_3^T\right) \le \sigma_{max}\|l_5\|\|\widetilde{W}\|\|d_w\|\|\tilde{h}_2\|\end{aligned} \tag{45}$$

where $l_5 = \rho_3^{-1}l_3 C_4$. By using Eqs. (41), (44), and by assuming that $\|u\| \le \bar{u}$; Eq. (46) is written as

$$\begin{aligned}\dot{L} \le -\alpha_1\|\tilde{h}_2\|^2 + \alpha_2\|\tilde{h}_2\| \\ + \|\tilde{h}_2\|\left(\alpha_3\|\widetilde{W}\| - \alpha_4\|\widetilde{W}\|^2\right)\end{aligned} \tag{46}$$

where $\alpha_1 = \frac{1}{2}\lambda_{min}(Q_1)$, $\alpha_2 = \|P_1\|\left\|\frac{P}{M}\right\|\bar{\delta}\bar{u}$, $\alpha_3 = \|P_1\|\left\|\frac{P}{M}\right\|\bar{u}\sigma_{max} + \sigma_{max}\|l_5\|\|d_w\| + W_{max}^*\|C_4\|$, and $\alpha_4 = \|C_4\|$ that all of them are positive. Besides, we can show that

$$\begin{aligned}&\alpha_3\|\widetilde{W}\| - \alpha_4\|\widetilde{W}\|^2 \\ &= -\left(\sqrt{\alpha_4}\|\widetilde{W}\| - \frac{\alpha_3}{2\sqrt{\alpha_4}}\right)^2 + \frac{\alpha_3^2}{4\alpha_4} \le \frac{\alpha_3^2}{4\alpha_4} = \beta_1, \\ &\beta_1 > 0\end{aligned} \tag{47}$$

Now, someone may rewrite Eq. (46) as

$$\dot{L} \le -\alpha_1\|\tilde{h}_2\|^2 + (\alpha_2 + \beta_1)\|\tilde{h}_2\| \tag{48}$$

so $\|\tilde{h}_2\|$ and $\|\tilde{z}_2\|$ are ultimately bounded because in the region $H = \left\{\tilde{h}_2 \middle| \|\tilde{h}_2\| \ge \frac{\alpha_2+\beta_1}{\alpha_1}\right\}$, $\dot{L}$ is negative hence the system energy is decreased.

2.3 Designing adaptive FTCS

Here, after estimating the residual efficiency of the damper, the control force is considered to decrease the effects of the damper power degradation as

$$u = \left(diag\left(\hat{f}_d\right)\right)^{-1}(-k\hat{x}) \tag{49}$$

where k is feedback gain.

The equation of the system is as

$$\dot{x} = Ax + B_1\ddot{x}_g + B_2(diag(f_d)u) \tag{50}$$

Therefore, by substituting Eq. (49) into Eq. (50), when $\hat{x}$ follows x, the equation of the system is as follows

$$\dot{x} = A^* x + B_1 \ddot{x}_g \tag{51}$$

where $A^* = A - B_2 k$. k is designed by LQR method so that A^* is Hurwitz thus the system is stable. Fig. 3 exhibits the flow chart of the above-introduced scheme.

3. Evaluation of proposed method

Here, a benchmark scaled numerical model of a three-story building structure is used to evaluate the proposed method. As illustrated in Fig. 4, an MR damper, a velocity sensor, and a displacement sensor are placed on each floor (Wang *et al*. 2009, Larbah and Patton 2010). The objective of numerical simulation is to evaluate the capacity of the FDI algorithm to isolate and identify faults. The inclusion of two sensors per floor rather than one accelerometer complicates the process. Furthermore, the structure's numerical model is a model of a laboratory structure and in the laboratory, the velocity and displacement can be measured by using an electrodynamic velocity sensor and linear variable differential transformer (LVDT) on each floor, respectively. The response of the building is studied under the El Centro record with PGA scaled to 1 m.s^{-2}. The MR dampers are type MRF-04K and Bouc–Wen model simulates their hysteretic behavior. The maximum capacity and required power are 20 kN and 50 W, respectively and the damper length and mass are 0.5 m and 50 kg, respectively. The selected parameters for Bouc–Wen model are described in Table 1. The damper force is calculated by Eq. (52) and z that represents MR damper's hysteretic behavior, is obtained by Eq. (53) as follows (Fallah and Taghikhany 2015)

$$F_{MR} = c_0 \dot{x} + k_0 (x - x_0) + \alpha z \tag{52}$$

$$\dot{z} = -\gamma |\dot{x}| z |z|^{n-1} - \beta \dot{x} |z|^n + A \dot{x} \tag{53}$$

where $\dot{x}$ is the damper relative velocity and x is the

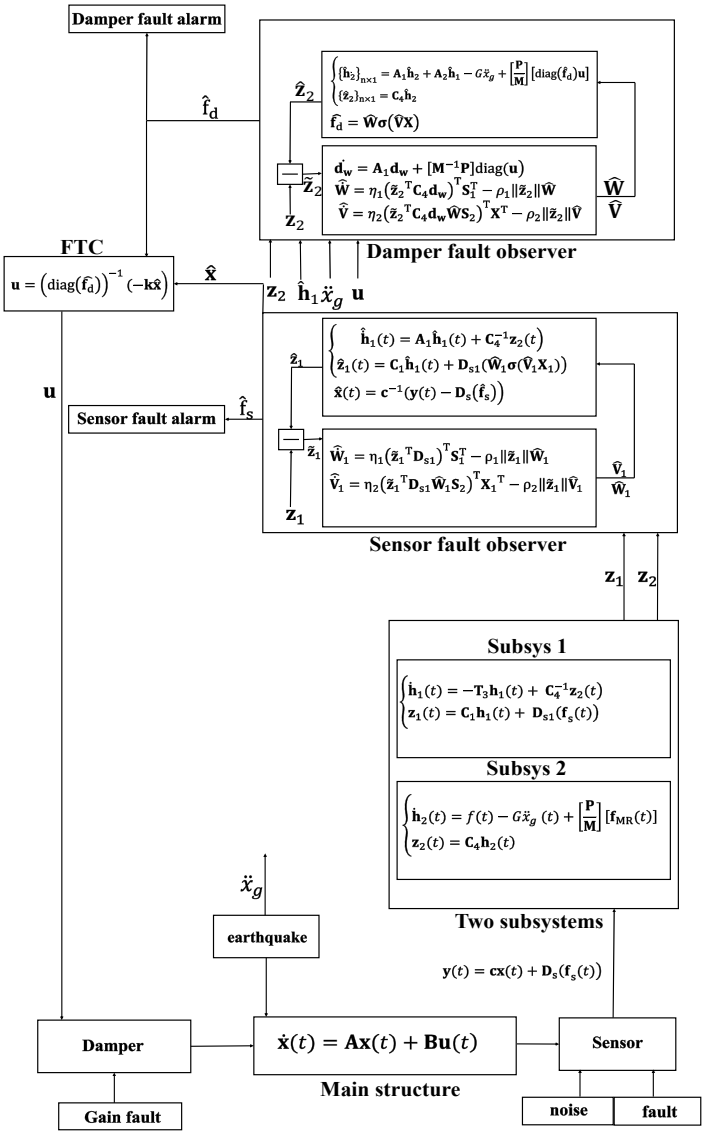

Fig. 3 Flow chart of the proposed strategy

Table 1 Parameters of the Bouk-Wen model (Fallah and Taghikhany 2015)

c_{0a} (N.s/cm)	c_{0b} (N.s/cm.V)	k_0 (N/cm)	x_0 (cm)	α_a (kN/cm)	α_b (kN/cm.V)	γ (cm^{-2})	β (cm^{-2})	n	A
80	15	10	18.6	2.1	1.7	30	30	2	60

Table 2 Distribution fault and transform matrices for benchmark model

Sensor fault distribution vector	State-space coordinate transformation matrix
$D_S=\begin{bmatrix}-1\\0\\0\\1\\0\\0\end{bmatrix}$	$T=\begin{bmatrix}1&0&0&0&0&0\\0&1&0&0&0&0\\0&0&1&0&0&0\\1&-0.43&0&1&0&0\\0&1.03&-0.38&0&1&0\\0&-0.38&0.6&0&0&1\end{bmatrix}$

Output transformation matrices

$$S_0=\begin{bmatrix}1.93&0.3&0.42&0.93&1.07&1.03\\-0.3&1.39&0&-0.3&-1.03&-0.37\\-0.42&0&1.39&-0.42&-0.35&-0.89\\2.78&0.30&0.42&2.78&2.23&2.12\\2.61&1.03&0.35&2.61&3.01&2.5\\2.32&0.37&0.89&2.32&2.45&3.04\end{bmatrix}\quad S'=\begin{bmatrix}1&0&0&0.03&-0.26&-0.15\\0&1&0&-0.64&1.07&-0.31\\0&0&1&0.00&-0.37&0.59\\0&0&0&1&0&0\\0&0&0&0&1&0\\0&0&0&0&0&1\end{bmatrix}$$

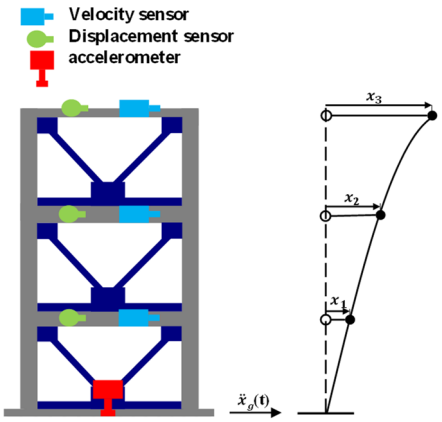

Fig. 4 The selected three-story benchmark structure, dampers and sensors

damper displacement. c_0 and α are as

$$c_0 = c_{0a} + c_{0b}u_{MR} \tag{54}$$

$$\alpha = \alpha_a + \alpha_b u_{MR} \tag{55}$$

where u_{MR} is the applied voltage. Since the controller calculates the desired control force, the inverse model of the damper is used to calculate the desired voltage which corresponds to the force as Eq. (56)

$$u_{MR} = \frac{F_{MR} - c_{0a}\dot{x} - \alpha_a z}{c_{0b}\dot{x} + \alpha_b z} \tag{56}$$

The DNN of the damper fault observer is pre-trained by using the behavior of the control system with the intact dampers under two far-field ground motions (Hachinohe (1968) and Mexico City (1984)) and two near-field records (Kobe (1995) and Northridge (1994)). The peak ground acceleration of far and near-field records were scaled to 1 $m.s^{-2}$ and 2 $m.s^{-2}$, respectively. The pre-trained weights are used as the initial weights of DNN in the online FDI.

The matrix of the sensor fault distribution (D_S), the state-space coordinate transformation (T), and the output transformation matrices (S', S_0) for the model are shown in Table 2. The DNNs' learning parameters are selected by trial and error considering the convergence speed.

The number of neurons in the input and output layers is equal to the number of input and output variables, respectively. Here, the structure's state is considered as the input variable and the control devices' faults are assumed as the output variables. By increasing the neuron number for the hidden layer, the network's capability will be increased in estimating a function; however, the over-training decreases the network predictive power (Smith and Gupta 2003). The hidden layer's neuron number is problem-dependent. For example, if the network will compress the data, it must have a hidden layer with a smaller neuron number than the input layer. Besides, noise and earthquake stimulation affect DNN's estimates. When the system is healthy, noise makes the output of the sensor fault observer's DNN not zero (zero means that the sensors are fault-free). Furthermore, affected by earthquake stimulation, the output of the damper fault observer is not one (one means that the dampers are fault-free) when dampers are healthy. In these conditions, the fault observer warns of a fault mistakenly. So, a threshold is set to prevent the wrong fault alarm. Monte Carlo method is used to determine the warning threshold to declare a fault if the estimated fault exceeds it (Abdollahi 2017).

An acceptable procedure is initially selecting the hidden layer's neuron number equal to half of the input data number. Then increase or decrease this number according to the training error (Hajian and Styles 2018). In this regard, the DNN used in the sensor fault observer is assumed with 10 neurons in the input layer, 3 neurons in the hidden layer

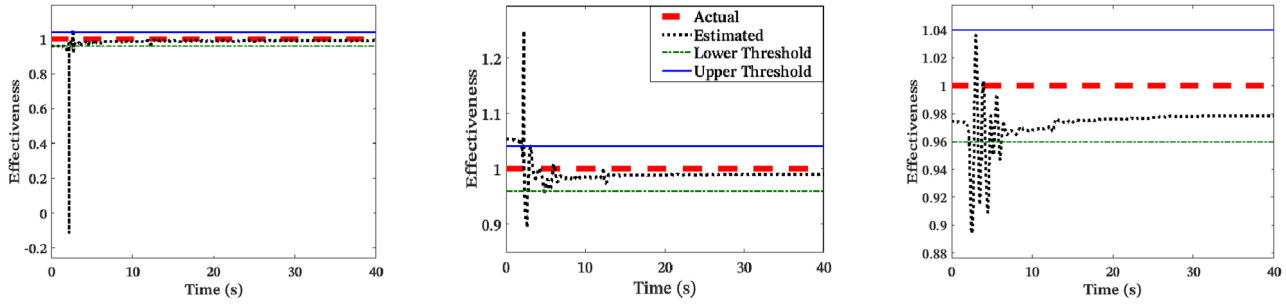

(a) The first story (b) The second story (b) The second story

Fig. 5 Actual and estimated dampers' effectiveness in the healthy case and fault alarm thresholds

and 1 neuron in the output layer. The learning parameters for this DNN are selected as $\eta_1 = \eta_2 = 20$, $\rho_1 = \rho_2 = 10^{-6}$, and the warning threshold of the fault is ±0.02. The damper fault observer has 10 neurons in the input layer, 10 neurons in the hidden layer and 3 neurons in the output layer. Its learning parameters are $\eta_3 = \eta_4 = 0.03$ and $\rho_3 = \rho_4 = 10^{-6}$. Fig. 5 shows the output of the damper fault observer's DNN in the healthy condition. As seen, the fault alarm thresholds were selected 0.96 as the lower threshold and 1.04 as the upper threshold. That is, when the efficiency of a damper exceeds them, the observer warns of a fault in the damper. Following algorithm convergence, the estimated value of the damper faults remains within the prescribed bounds in the healthy situation. This figure illustrates the robustness of the proposed FDI method to uncertainty, including noise and earthquake.

Here, we investigate the effectiveness of the proposed strategy using the following two fault scenarios;

1) In first scenario, different bias faults assumed in the sensors on the first floor. A 2 m.s^{-1} deviation in the velocity sensor's output ($f_s = 2\,\mathrm{m.s^{-1}}$) and a 2 m deviation in the displacement sensor's output ($f_s = -2\,\mathrm{m}$) from their respective true values. Additionally, on the second floor, a multiplicative fault is considered in MR damper which limits its capacity to 40% of the force commanded by the controller ($f_d = 0.4$). In this scenario, the sensors' outputs experience abnormal spikes and damper's capacity drops to 40% of its nominal condition.
2) In this scenario, bias faults are again assumed only in the sensors on the first floor, however with smaller magnitudes to evaluate the FDI algorithm's ability to detect and isolate minor defects. The bias faults for the velocity and displacement sensors are set at 0.04 $\mathrm{m.s^{-1}}$ and -0.04 m respectively. Additionally, to assess the method's performance in the presence of multiple faulty dampers, simultaneous abrupt and time-varying multiplicative faults are assumed in the dampers of the second and third floors, respectively, while the first floor damper is healthy. The damper faults are defined as $f_d = [1,\ 0.5,\ 0.5 + e^{-t}]^T$. The method's effectiveness in handling time-varying faults is explored. In the first scenario, Fig. 6 shows the actual and the identified sensor faults on the first floor. As seen, the fault in displacement and velocity sensors are very well tracked and the estimated values are equal to the assumed values. While sensors have faults, Fig. 7 shows that the estimated time history displacement and velocity on the first floor are in plausible agreement with the actual responses. Concurrent with the sensors' faults in this scenario, the damper on the second floor is assumed faulty as exhibited in Fig. 8. As seen, the damper fault observer can track the fault and after a few seconds, it approaches the actual value. The figures compellingly demonstrate the FDI algorithm's ability to accurately distinguish between sensor and damper fault types, identify their values, and effectively restore precise sensor output. Fig. 9 compares the controller's force in the faulty case with the healthy case. This figure illustrates the controller's fault-tolerant strategy for damper failures. It can be observed that in the faulty situation, the controller increases the control force commanded to the damper to accommodate the effects of its malfunctioning. As can be seen, the variance and the mean of the healthy and faulty forces are different. This is attributable to the multiplicative effect of the damper fault.

As described in the second scenario, sensor and damper faults are taking place concurrently. Fig. 10 demonstrates the capability of the suggested sensor fault observer to estimate the sensors' faults on the first floor in the second scenario, despite the minimal influence of these faults on the building's overall behavior. Fig. 11 shows that the DNN-based sensor fault observer can exactly estimate the model's states in this scenario. Fig. 12 shows the efficiency of the damper fault observer in estimating the assumed multiplicative faults in three different dampers. As seen in this figure, the estimated fault for the healthy first floor damper remains below the failure alarm threshold upon method convergence, preventing a false alarm (Fig. 12(a)), the abrupt fault on the second floor's damper is identified after three seconds (Fig. 12(b)) and also the damper fault observer tracks very well the time variation of the fault on the third floor's damper (Fig. 12(c)). These results confirm that the proposed FDI algorithm consistently delivers ideal performance even when confronted with simultaneous failures of multiple sensors and dampers, irrespective of whether these failures occur abruptly or gradually.

Here, our controller's ability to compensate for the

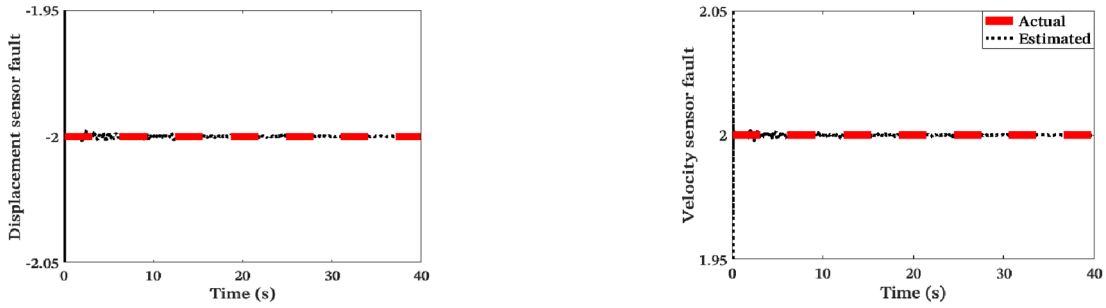

(a) The first story displacement sensor (b) The first story velocity sensor

Fig. 6 Actual and estimated faults (scenario 1)

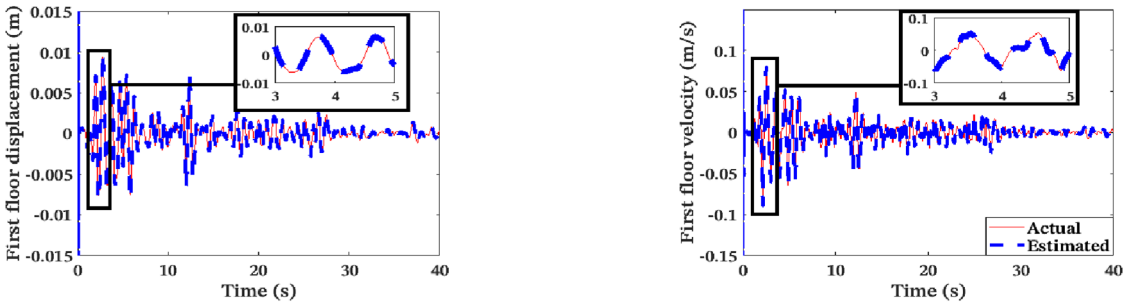

(a) The first story displacement (b) The first story velocity

Fig. 7 Actual and estimated responses (scenario 1)

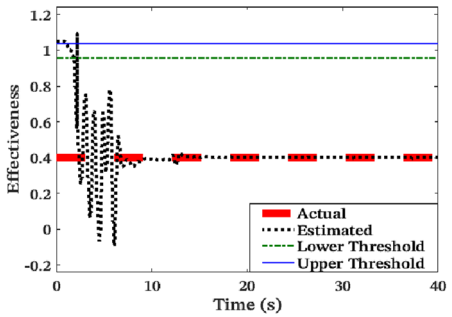

Fig. 8 Actual and estimated faults on the second story damper (scenario 1)

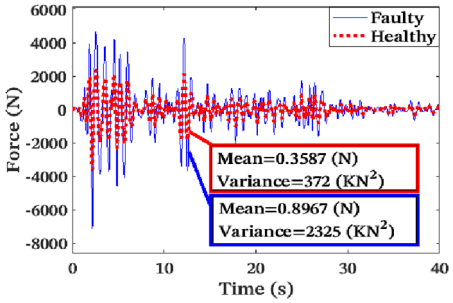

Fig. 9 The time history of the calculated force of the controller on second floor in healthy and faulty condition (scenario1)

effects of the damper faults is evaluated. In this regard, Fig. 13 compares maximum displacements, inter-story drift ratios and accelerations for the floor levels of the structure and three different controllers:

a) Model reference adaptive controller (MRAC) with control law as $u = -\hat{k}x$, where by employing the adjustable gain $(\hat{k})$, the controller compels the plant to emulate the desired reference model dynamics. The adaptation rules are as $\hat{k}_i = -\gamma_i B_{2i}^T P_2 e x^T$ $(i = 1,2,\dots,m)$, where γ_i is the adjustment rate, P_2 is a positive-definite matrix, which satisfies the Lyapunov equation as $A^T P_2 + P_2 A = -Q_2$, and e is the difference between the state of the reference model and the controlled structure. Here, the building's health status serves as the reference model, $\gamma_i = 20$, and $P_2 = 10^{10} I$ (Naderpoor Shad and Taghikhany 2022),

b) LQR controller in which $R = 10^{-9} I$ and $Q = I$ (Naderpoor Shad and Taghikhany 2022),

c) The proposed fault-tolerant controller in two scenarios as below;

i) with damper faults as scenario 1 (Fig. 13(a))

ii) with damper faults as scenario 2 (Fig. 13(b)).

The figure demonstrates that both the MRAC and the proposed controller outperform the classic LQR approach in reducing all three types of the responses of the structure.

The proposed controller further enhances performance by reducing maximum displacement response and maximum inter-story drift ratio by 10% and 21% compared to the LQR method, respectively and by 9% and 15% relative to the MRAC, respectively. There is little difference in acceleration between the suggested and MRAC methods.

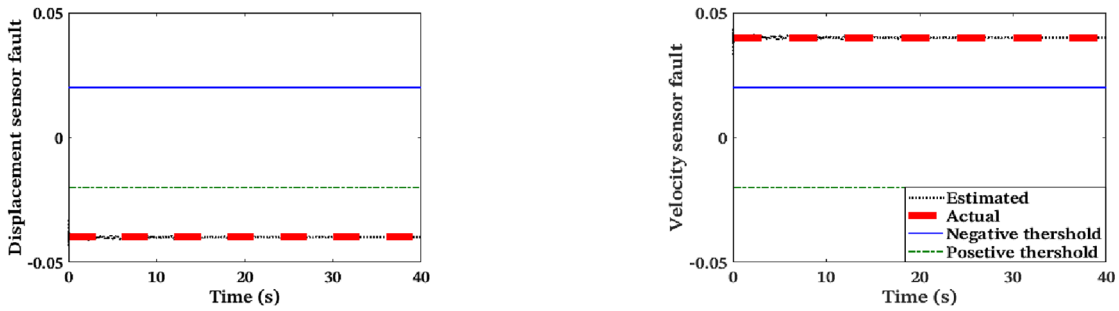

(a) The first story displacement sensor (b) The first story velocity sensor

Fig. 10 Actual and estimated faults (scenario 2)

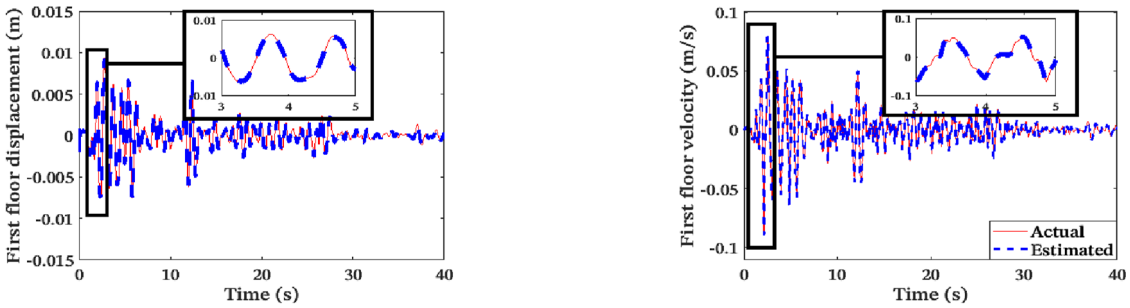

(a) The first story displacement (b) The first story velocity

Fig. 11 Actual and estimated responses (scenario 2)

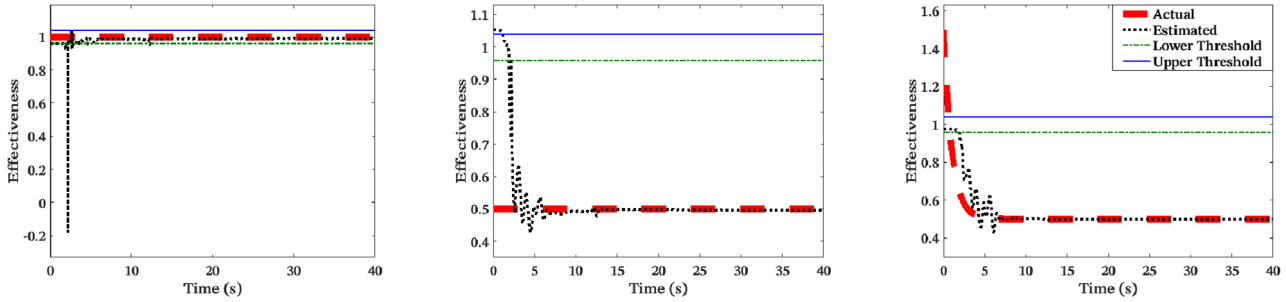

(a) The first story damper (b) The second story damper (c) The third story damper

Fig. 12 Actual and estimated faults (scenario 2)

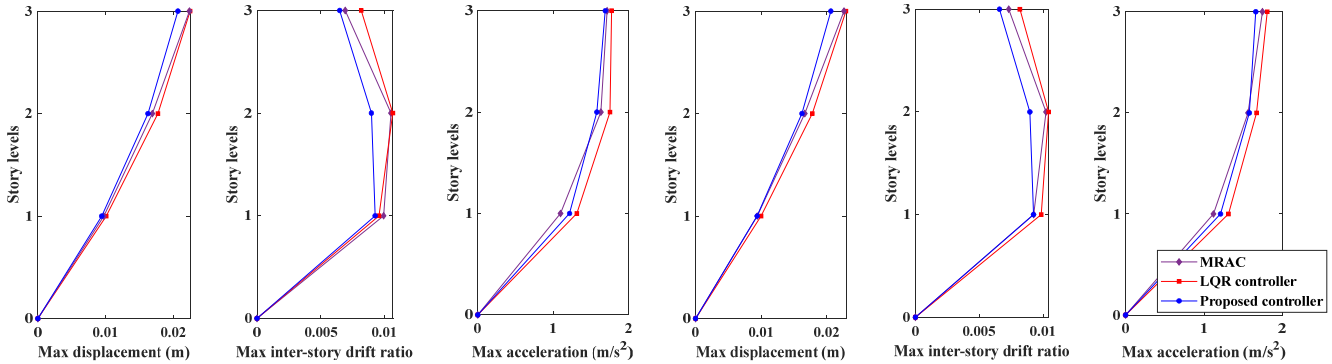

(a) Scenario 1 (b) Scenario 2

Fig. 13 The vertical profile of the peak responses

These findings underscore the effectiveness of the suggested controller in mitigating the impact of damper defects.

4. Conclusions

In this paper, a scheme was suggested for AFTC of building structures when besides that the sensors produce false data, the dampers lose a percentage of their efficiency. The assumed sensor malfunction only changes the average of the actual signal, but the presumed damper fault also affects its variance. However, in a few studies, these faults of the control tools called additive and multiplicative have been considered together. To this goal, firstly, sensor and damper faults were decoupled. Then a DNN-based sensor fault observer was designed to estimate "the sensor faults + the structure states" and a damper fault observer based on DNN was also introduced to estimate "the damper faults". Eventually, a fault-tolerant controller compensated the approximated damper fault effects. In this article, the damper fault observer's DNN was pre-trained offline by using the healthy situation of the system under various earthquakes. Pre-trained weights were used as the initial weights of the DNN in online FDI to increase the learning speed and improve the online estimation behavior. Lastly, the benefit of the proposed method was confirmed by simulating different fault scenarios.

For future research, it is suggested that the algorithm be developed for faults other than additive and multiplicative types.

References

Abdollahi, M. (2017), "Fault- tolerant control strategies for a class of Euler-Lagrange nonlinear systems subject to simultaneous sensor and actuator faults", *Concordia University*.

Balzano, L. and Nowak, R. (2007), "Blind calibration of sensor networks", *Proceedings of the 6th International Conference on Information Processing in Sensor Networks*, pp. 79-88. https://doi.org/10.1145/1236360.1236372

Bozorgvar, M. and Zahrai, S.M. (2019), "Semi-active seismic control of a 9-story benchmark building using adaptive neural-fuzzy inference system and fuzzy cooperative coevolution", *Smart Struct. Syst., Int. J.*, **23**(1), 1-14. https://doi.org/10.12989/sss.2019.23.1.001

Chen, P.C., Sugiarto, B.J. and Chien, K.Y. (2021), "Performance-based optimization of LQR for active mass damper using symbiotic organisms search", *Smart Struct. Syst., Int. J.*, **27**(4), 705-717. https://doi.org/10.12989/sss.2021.27.4.705

Fallah, A.Y. and Taghikhany, T, (2015), "Sliding mode fault detection and fault-tolerant control of smart dampers in semi-active control of building structures", *Smart Mater. Struct.*, **24**(12), p. 125030. https://doi.org/10.1088/0964-1726/24/12/125030

Gao, K., Chen, Z.D., Weng, S., Zhu, H.P. and Wu, L.Y. (2022), "Detection of multi-type data anomaly for structural health monitoring using pattern recognition neural network", *Smart Struct. Syst., Int. J.*, **29**(1), 129-140. https://doi.org/10.12989/sss.2022.29.1.129

Hajian, A. and Styles, P. (2018), *Application of soft computing and intelligent method in geophysics*, Springer International Publishing.

Hosseini, A., Taghikhany, T. and Yeganeh Fallah, A. (2018), "Direct adaptive algorithm for seismic control of damaged structures with faulty sensors", *J. Vib. Control*, **24**(24), 5854-5866. https://doi.org/10.1177/1077546316687958

Jung, H.J., Spencer Jr, B.F. and Lee, I.W. (2003), "Control of seismically excited cable-stayed bridge employing magnetorheological fluid dampers", *J. Struct. Eng.*, **129**(7), 873-883. https://doi.org/10.1061/(ASCE)0733-9445(2003)129:7(873)

Larbah, E and Patton, R.J. (2010), "Fault tolerant plug and play vibration control in building structures", *Proceeding of the 49th IEEE Conference on Decision and Control* (*CDC*). https://doi.org/10.1109/CDC.2010.5717781

Li, Y. and Li, J. (2019), "Overview of the development of smart base isolation system featuring magnetorheological elastomer", *Smart Struct. Syst., Int. J.*, **24**(1), 37-52. https://doi.org/10.12989/sss.2019.24.1.037

Li, L., Song, G. and Ou, J. (2011), "DNN based fault tolerant control of nonlinear structural vibration with actuator faults", *Adv. Struct. Eng.*, **14**(5), 871-879. https://doi.org/10.1260/1369-4332.14.5.871

Lin, T.K., Lu, L.Y. and Chen, C.J. (2018), "Semi-active leverage-type isolation system considering minimum structural energy", *Smart Struct. Syst., Int. J.*, **21**(3), 373-387. https://doi.org/10.12989/sss.2018.21.3.373

Naderpoor Shad, P. and Taghikhany, T. (2022), "Seismic adaptive control of building structures with simultaneous sensor and damper faults based on dynamic neural network", *Comput.-Aided Civil Infrastr. Eng.*, **37**(11), 1402-1416. https://doi.org/10.1111/mice.12805

Ni, K., Ramanathan, N., Chehade, M.N.H., Balzano, L., Nair, S., Zahedi, S., Kohler, E., Pottie, G., Hansen, M. and Srivastava, M. (2009), "Sensor network data fault types", *ACM Transactions on Sensor Networks* (*TOSN*), **5**(3), 1-29. https://doi.org/10.1145/1525856.1525863

Oh, B.K., Glisic, B. and Park, H.S. (2021), "Convolutional neural network-based damage detection method for building structures", *Smart Struct. Syst., Int. J.*, **27**(6), 903-916. https://doi.org/10.12989/sss.2021.27.6.903

Ossmann, D. and Varga, A. (2013), "Detection and identification of loss of efficiency faults of flight actuators", In: *2013 Conference on Control and Fault-Tolerant Systems* (*SysTol*), pp. 19-24. https://doi.org/10.1109/SysTol.2013.6693841

Ramanathan, N., Balzano, L., Burt, M., Estrin, D., Harmon, T., Harvey, C., Jay, J., Kohler, E., Rothenberg, S. and Srivastava, M. (2006), "Rapid deployment with confidence: Calibration and fault detection in environmental sensor networks", *Center for Embedded Network Sensing*.

Sharma, A., Golubchik, L. and Govindan, R. (2007), "On the prevalence of sensor faults in real-world deployments", In: *2007 4th Annual IEEE Communications Society Conference on Sensor, Mesh and Ad Hoc Communications and Networks*, pp. 213-222. https://doi.org/10.1109/SAHCN.2007.4292833

Shen, Q., Jiang, B. and Shi, P. (2017), "Adaptive fault tolerant control against actuator faults", *Int. J. Adapt. Control Signal Process.*, **31**(2), 147-162. https://doi.org/10.1002/acs.2689

Smith, K.A. and Gupta, J.N. (2003), "Neural networks in business: Techniques and applications", IGI Global.

Talebi, H.A. and Khorasani, K. (2012), "A neural network-based multiplicative actuator fault detection and isolation of nonlinear systems", *IEEE Transact. Control Syst. Technol.*, **21**(3), 842-851. https://doi.org/10.1109/TCST.2012.2186634

Talebi, H.A., Khorasani, K. and Tafazoli, S. (2008), "A recurrent neural-network-based sensor and actuator fault detection and isolation for nonlinear systems with application to the satellite's attitude control subsystem", *IEEE Transact. Neural Networks*, **20**(1), 45-60. https://doi.org/10.1109/TNN.2008.2004373

Tudon-Martinez, J.C. and Morales-Menendez R. (2015), "Adaptive vibration control system for MR damper faults", *Shock Vib*. https://doi.org/10.1155/2015/163694

Utami, D., Mazlan, S.A., Imaduddin, F., Nordin, N.A., Bahiuddin, I., Abdul Aziz, S.A., Mohamad, N., Choi, S.B. (2018), "Material characterization of a magnetorheological fluid subjected to long-term operation in damper", *Materials*, **11**(11), p. 2195. https://doi.org/10.3390/ma11112195

Wang, Y., Lynch, J.P. and Law, K.H. (2009), "Decentralized $\mathscr{H}\infty$ controller design for large-scale civil structures", Earthquake *Eng*. *Struct*. *Dyn*., **38**(3), 377-401. https://doi.org/10.1002/eqe.862

Xu, Y.L., Qu, W.L. and Ko, J.M. (2000), "Seismic response control of frame structures using magnetorheological/ electrorheological dampers", *Earthq*. *Eng*. *Struct*. *Dyn*., **29**(5), 557-575. https://doi.org/10.1002/(SICI)10969845(200005)29:5%3C557::AID-EQE922%3E3.0.CO;2-X

Zhu, B., Lin, W., Zhan, Q., Sun, W., Hayat, T. and Alsaadi, F. (2015), "Active fault tolerant control of buildings for seismic loads in finite frequency domain", *J*. *Franklin Inst*., **352**(10), 4247-4262. https://doi.org/10.1016/j.jfranklin.2015.06.013